Engineering Alkaline-Stable Barley Stripe Mosaic Virus-Like Particles for Efficient Surface Modification

Akash J. Vaidya[a‡], *Mruthula Rammohan*[a‡], *Yu-Hsuan Lee*[b‡], *Kok Zhi Lee*[c, d‡], *Che-yu Chou*[b], *Zachary Hartley*[e], *Corren A. Scott*[b], *Rachel G. Susler*[b], *Longfei Wang*[f], *L. Sue Loesch-Fries*[f], *Michael T. Harris*[b], *Kevin V. Solomon*[a,c,d,g*]

AUTHOR ADDRESSES

[a] 150 Academy St, Department of Chemical & Biomolecular Engineering, University of Delaware, Newark, DE, 19716, USA

[b] 480 Stadium Mall Drive, School of Chemical Engineering, Purdue University, West Lafayette, IN 47907, United States

[c] 225 South University Street, Agricultural & Biological Engineering, Purdue University, West Lafayette, IN 47907-2093, United States

[d] 1203 West State Street, Bindley Bioscience Center, Purdue University, West Lafayette, IN 47906, United States

[e] 915 West State Street, Plant Genetics, Breeding and Biotechnology Program, Department of Agronomy, Purdue University, West Lafayette, IN 47907, United States

[f] 915 West State Street, Department of Botany and Plant Pathology, Purdue University, West Lafayette, IN 47907, United States

[g] 500 Central Drive, Laboratory of Renewable Resources Engineering (LORRE), Purdue University, West Lafayette, IN, 47907-2022, United States

[‡] Equal contribution

[*] Corresponding author: kvs@udel.edu

KEYWORDS

biotemplate, Barley stripe mosaic virus (BSMV), VLP, Caspar carboxylate cluster, *E. coli*, surface functionalization

ABSTRACT

Viruses and virus-like particles are powerful templates for materials synthesis because of their capacity for precise protein engineering and diverse surface functionalization. We recently developed a recombinant bacterial expression system for the production of barley stripe mosaic virus-like particles (BSMV VLPs). However, the applicability of this biotemplate was limited by low stability in alkaline conditions and a lack of chemical handles for ligand attachment. Here, we identify and validate novel residues in the BSMV Caspar carboxylate clusters that mediate virion disassembly through repulsive interactions at high pH. Point mutations of these residues to create attractive interactions that increase rod length ~2 fold, with an average rod length of 91 nm under alkaline conditions. To enable diverse chemical surface functionalization, we also introduce reactive lysine residues at the C-terminus of BSMV coat protein, which is presented on the VLP surface. Chemical conjugation reactions with this lysine proceed more quickly under alkaline conditions. Thus, our alkaline-stable VLP mutants are more suitable for rapid surface functionalization of long nanorods. This work validates novel residues involved in BSMV VLP assembly and demonstrates the feasibility of chemical functionalization of BSMV VLPs for the first time, enabling novel biomedical and chemical applications.

1. Introduction

Plant viruses and virus-like particles (VLPs) are attractive templates for the synthesis of well-defined nanomaterials with diverse applications [1]. As protein bionanoparticles that replicate in plants, they can be scalably and sustainably produced. The vast majority of plant viruses are nonenveloped, and their lack of lipid content confers broad temperature stability [2,3]. Coat proteins of various plant viral species can even assemble without their native genomes, yielding non-infectious VLPs [4]. Having evolved to infect plant hosts, various plant viruses and VLPs have high biocompatibility that further extends their range of applicability to medical applications such as vaccine and drug delivery [5]. They also exhibit highly ordered nanoscale structures with diverse geometries composed of hundreds to thousands of capsid proteins, providing an opportunity for high-density surface display. Decoration with small-molecule chemicals, polymers, peptides, proteins, metals, and other ligands enabled the widespread application of plant viruses in (bio)sensing, catalysis, energy, and medicine [6–8].

Rod-shaped plant viruses such as tobacco mosaic virus (TMV), the first virus ever discovered, are particularly popular and well-characterized as nanomaterial templates [9]. This cylindrical virus consists of a single capsid protein that self-assembles via protein::protein and nucleic acid::protein interactions [10]. Viral capsid proteins first assemble into washer-like structures with a diameter of ~20 nm via hydrophobic and electrostatic interactions encoded within their structure. These washers stack into nanorods to encapsidate viral genomic RNA and complete the multi-stage assembly process. Once the rods enter host cells, viral capsid proteins repel each other to disassemble the rods and restart the viral replication cycle. The transition between self-assembly and self-repulsion is mediated in TMV by a cluster of negatively charged carboxylate residues within the capsid protein or Caspar Carboxylate Cluster (CCC) motif [11–13]. These repulsive interactions can be neutralized through proton or calcium ion-mediated charge shielding, allowing viral assembly. However, under higher pH or low Ca^{2+}, such as that experienced intracellularly, these repulsive interactions are unshielded and the particles disassemble [11,14]. Similar CCC-forming residues were proposed for barley stripe mosaic virus (BSMV), another rod-shaped plant virus of the *Virgaviridae* family with high structural similarity to TMV, based on cryo-electron microscopy (EM) [15,16]. The near-atomically resolved cryo-EM structures further revealed that the C-termini of both viruses are exposed on the particle surface. This information is

essential for incorporating functional moieties onto the surface of TMV and BSMV, and the latter is quickly drawing attention as an efficient biotemplate [17].

Various chemical and bioconjugation strategies have been established for the surface functionalization of rod-shaped plant viral particles, each with unique advantages and disadvantages [18]. Direct fusion to the surface-exposed C-terminus is the most straightforward route for peptide and protein display, which is common when diverse biological functionalities are desired. However, this approach is heavily restricted by the need to preserve host infectivity for *in planta* production. Apart from a single exception in which TMV was fused to a small, 133-residue protein [19], direct fusion is typically limited to short peptides below ~20 residues long [20,21]. Even the insertion of a single residue can interfere with plant viral replication and stability. For example, significant screening and optimization were used to generate TMV mutants with surface-exposed lysine residues; and all successful clones contained extra acidic residues to balance out the positive charge of lysine's amino side chain [22]. Once the lysine-displaying mutants were generated, they enabled facile surface functionalization via chemical coupling and indirect bioconjugation through the binding of streptavidin to biotinylated VLPs [23]. Nonetheless, the requirement of plant host infectivity clearly limits viral engineering. To address this issue, we recently established the production of noninfectious BSMV VLPs in bacteria, allowing for faster production times and decoupling viral fitness or infectivity from production [24]. Bacterially produced VLPs can be used for templating with similar efficiency to *in planta* virus [24] and are more amenable to engineering that would introduce desired properties that would otherwise reduce infectivity (e.g., pH stability/reduction of infectivity at neutral pHs) [25]. Thus, the stage is set for further engineering BSMV VLPs with targeted physicochemical and biological properties.

Engineering rod-shaped plant VLPs with improved stability at alkaline pH is crucial for important functionalization approaches including metal mineralization and chemical modification. For example, buffer pH near and above 9 greatly accelerates the electroless deposition of ruthenium oxides for catalytic and energy storage applications [26]. This pH range also favors electroless deposition of other metals and alloys, including nickel-phosphorous [27]. However, since viral particles are typically unstable in this environment, adsorption of these metals typically requires extra processing steps, such as platinum or palladium pre-activation [28]. Particle instability in alkaline conditions is also troublesome for functionalization via organic chemical reactions. For example, the electrophilic aromatic substitution of diazonium salts onto tyrosine

phenols requires pH values between 9 and 10. This is a popular and highly efficient reaction that can be used to modify rod-shaped plant viruses with diverse functional groups [29]. Similarly, the rate constant is over 12 times higher at pH 9.5 than at pH 6.5 for the conjugation reaction between various isothiocyanates and a cysteine-functional protein [30]. Particle surface-exposed lysine residues are another favorable site for chemical couplings to TMV, as the highly nucleophilic amine group readily attacks esters, acids, maleimides, isocyanates, and other electrophiles. However, amine nucleophilicity drops dramatically upon protonation, primarily at pH values below its pKa of ~9 [31]. Unfortunately, CCC-mediated repulsive interactions destabilize rod-shaped plant viruses in alkaline conditions far below this value [10]. Enhancing the pH stability of BSMV VLPs would therefore enable important engineering opportunities for numerous applications.

To maintain the assembly of BSMV capsid protein in a wider range of processing conditions, control and enhancement of its self-assembly are needed. Point substitution of CCC residues improved the pH stability of TMV rods by neutralizing their repulsive interactions, but this has never been attempted with BSMV [32,33]. We hypothesized that neutralizing repulsive interactions between selected negative carboxylates within the CCC would similarly stabilize the assembly of BSMV capsid proteins and enhance its pH stability. While a putative CCC for BSMV has been proposed by Clare et al. based on crystallization data [15], these sites are yet to be validated. In this paper, we assess these candidates and experimentally validate novel CCC residues. In doing so, we generate alkaline stable BSMV VLPs and further functionalize them with reactive handles for subsequent chemical conjugation. Our work validates the engineering flexibility of BSMV-derived VLPs and establishes chemical strategies for surface modification and functionalization for diverse applications.

2. Materials and methods

2.1 BSMV Protein Crystal Structure Alignment

Analogous CCC candidate residues to those validated in TMV were identified via sequence structural alignment. The capsid proteins of TMV (PDB: 2xea) and BSMV (PDB: 5a7a) were structurally aligned via TM-align (version 20190822) with the default setting [34]. TMV-validated CCC residues E50 and D77 were used to find the corresponding residues on BSMV capsid protein

based on the structural proximity of negatively-charged residues. The individual and overlay structures were downloaded from TM-align output and visualized via pymol. The putative candidate residues were then subjected to site-directed mutagenesis for experimental validation.

2.2 Cloning of BSMV Capsid Protein Mutants

E. coli strains and plasmids used in this study are listed in Table 1. All molecular biology manipulations were carried out according to standard practices [35]. BSMV CP CCC-mutants were made via site-directed mutagenesis [36]. Briefly, plasmid pET21-BSMV-CP [24] was amplified with Phusion DNA polymerase (Thermo Fisher Scientific, Waltham, MA. Cat. No: F530S) and mutagenic primers described in Table 2. Cleaned up reaction products were then digested with DpnI to remove unmutated plasmid before transformation into *E. coli*. The D101R mutant with an additional C-terminal lysine insertion was made through PCR from pET21-BSMV-CP-D101R with primers 199K 5'/199K 3'; the 3' primer contained a random codon inserted right before the stop codon and introduced AgeI sites downstream. pET21-BSMV-CP and insert were then digested with AgeI and XbaI to enable swapping of wildtype BSMV-CP and the BSMV-D101R/199K insertion mutant via standard recombinant biotechnology approaches [35]. Colonies were screened to identify one with a lysine-encoding codon inserted at the C-terminus. All constructs were verified via Sanger sequencing at Genewiz (South Plainfield, NJ).

Table 1. Strains and plasmids

Name	Relevant genotype	Vector backbone	Plasmid origin	Source
Strain				
BL21-CodonPlus(DE3)-RIPL	*E. coli* B F^- *ompT hsdS*(r_B^- m_B^-) *dcm*$^+$ Tet^r *gal* λ(DE3) *endA* Hte [*argU proL* Cam^r] [*argU ileY leuW* Strep/$Spec^r$	N/A	N/A	Agilent Technologies
Plasmid				
pET21-BSMV-CP	BSMV-CP-linker-OAS, *bla*	pET21-1cys-tmv-cp	pBR322	Lee *et al.*[24]
pET21-BSMV-CP-E37Q	BSMV-CP-E37Q- linker, *bla*			This study
pET21-BSMV-CP-E37R	BSMV-CP-E37R-linker, *bla*			
pET21-BSMV-CP-E62Q	BSMV-CP-E62Q-linker, *bla*			
pET21-BSMV-CP-D68N	BSMV-CP-D68N-linker, *bla*			
pET21-BSMV-CP-D70N	BSMV-CP-D70N-linker, *bla*			
pET21-BSMV-CP-D101N	BSMV-CP-D101N-linker, *bla*			
pET21-BSMV-CP-D101R	BSMV-CP-D101R-linker, *bla*			
pET21-BSMV-CP-D101K	BSMV-CP-D101K-linker, *bla*			
pET21-BSMV-CP-E62Q/D101N	BSMV-CP-E62Q/D101N-linker, *bla*			
pET21-BSMV-CP-D101R / 199K	BSMV-CP-E62Q/199K-linker, *bla*			

Table 2. DNA primers were used in this study. The modified nucleotides corresponding to the modified codons are in lowercase. Introduced AgeI sites are underlined.

Name	Sequences (5'>3')	Template	Used to construct
E37Q 5'	TGGTGGGTGCATGTAcAGGCCTGGAATAAGT	pET21-BSMV-CP	pET21-BSMV-CP-E37Q
E37Q 3'	ACTTATTCCAGGCCTgTACATGCACCCACCA		
E37R 5'	TGGTGGGTGCATGTAcgtGCCTGGAATAAGTTT	pET21-BSMV-CP	pET21-BSMV-CP-E37R
E37R 3'	AAACTTATTCCAGGCacgTACATGCACCCACCA		
E62Q 5'	CGCTCACAAGTAGCAcAGTATTTGGCTGCTT	pET21-BSMV-CP	pET21-BSMV-CP-E62Q and pET21-BSMV-CP-E62Q/D101N
E62Q 3'	AAGCAGCCAAATACTgTGCTACTTGTGAGCG		
D68N 5'	TATTTGGCTGCTTTGaATCGTGACCTTCCGG	pET21-BSMV-CP	pET21-BSMV-CP-D68N
D68N 3'	CCGGAAGGTCACGATtCAAAGCAGCCAAATA		
D70N 5'	GCTGCTTTGGATCGTaACCTTCCGGCTGACG	pET21-BSMV-CP	pET21-BSMV-CP-D70N
D70N 3'	CGTCAGCCGGAAGGTtACGATCCAAAGCAGC		
D101N 5'	AAATTTTTTCGTCTTaATAAACGTACAATCG	pET21-BSMV-CP	pET21-BSMV-CP-D101N and pET21-BSMV-CP-E62Q/D101N
D101N 3'	CGATTGTACGTTTATtAAGACGAAAAAATTT		
D101R 5'	AAATTTTTTCGTCTTcgTAAACGTACAATCGC	pET21-BSMV-CP	pET21-BSMV-CP-D101R
D101R 3'	GCGATTGTACGTTTAcgAAGACGAAAAAATTT		
D101K 5'	AAATTTTTTCGTCTTaaaAAACGTACAATCGCT	pET21-BSMV-CP	pET21-BSMV-CP-D101K
D101K 3'	AGCGATTGTACGTTTtttAAGACGAAAAAATTT		
199K 5'	GGAATTGTGAGCGGATAACA	pET21-BSMV-CP-D101R	pET21-BSMV-CP-199K
199K 3'*	TATTACCGGTTTAmnnTGCTTCCTCTGCATCTGG		

* M and N designate random A/C and A/T/G/C bases, respectively

2.3 BSMV Capsid Protein Expression

The BSMV-capsid protein expression plasmids were transformed into *E. coli* BL21-CodonPlus (DE3)-RIPL (Agilent Technologies, Santa Clara, CA. Cat. No.: #230280). The bacteria were streaked onto plates containing LB media plus 100 μg/ml ampicillin and 25 μg/ml chloramphenicol and incubated for 16-20 hours at 37 °C. Single colonies were selected, inoculated into LB broth, and incubated at 37 °C for 16-20 hours at 250 RPM. The liquid cultures were then diluted a hundred-fold in LB broth and incubated at 37 °C until an OD_{600} of 0.5. The cultures were induced with the addition of 0.1 mM isopropyl β-D-1-thiogalactopyranoside (IPTG) to express the BSMV capsid protein followed by incubation for 16 hours at room temperature (~23 °C) to express capsid protein. All BL21-CodonPlus (DE3)-RIPL liquid cultures or plates contained ampicillin (100 μg/ml) and chloramphenicol (25 μg/ml). Bacteria were collected by centrifugation at room temperature for 5 min at 6000 rpm. The pellet containing the bacteria was used directly for isolation of BSMV VLPs or stored at -80 °C.

2.4 BSMV-VLP Purification

Protein expression and purification for BSMV carboxylate residue mutants were performed as described previously [24]. In brief, BSMV VLPs were isolated from *E.coli* cell pellets by resuspension in BugBuster® Protein Extraction Reagent (MilliporeSigma, Burlington, MA) supplemented with Lysonase™ Bioprocessing Reagent (MilliporeSigma, Burlington, MA) as per the manufacturer protocol. Lysates were then incubated at room temperature for 10 min and centrifuged at 19,000 × g for 10 min to remove the insoluble lysates. VLPs were isolated from the soluble protein lysates by centrifugation at 64,000 × g at 4 ºC for 1 h. The isolated VLP pellets were resuspended in 10 mM Tris-HCl at pH 7 or pH 9 at 4 ºC.

In order to obtain pure BSMV-D101R/199K VLPs for further surface functionalization, a different purification protocol was followed. After the VLPs were isolated from *E.coli* using BugBuster® Protein Extraction Reagent and Lysonase™ Bioprocessing Reagent, the suspension was incubated for 15 min at room temperature on a shaker to lyse the cells. The lysis was followed by centrifugation at 21,000 × g for 15 min at 4 ºC to remove the insoluble lysates. The VLPs in the soluble protein lysates were pelleted by ultracentrifugation on a 25% (w/v) sucrose cushion at

30,000 rpm at 4 ºC for 3.5 h. The pellet was allowed to resuspend in 1x PBS at 4 ºC for 2 days, after which the suspension was passed through a 0.22 μm syringe filter for future use.

2.5 Verification of Capsid Protein Expression

To validate coat protein expression, cell lysates were analyzed on 14% polyacrylamide gels (Thermo Fisher Scientific, Waltham, MA. Cat. No.: XP04200BOX). 14 µl of protein lysate was mixed with an equal volume of 2X Tris-glycine SDS Sample Buffer (Thermo Fisher Scientific, Waltham, MA. Cat. No.: LC2676) and supplemented with 2 µl of 1M DTT (Thermo Fisher Scientific, Waltham, MA. Cat. No.: AC426380100). Samples were then incubated at 85°C for 5 minutes to denature the proteins. Samples were then placed on ice for 5 minutes before electrophoresis. PageRuler™ Plus Prestained Protein Ladder (Thermo Fisher Scientific, Waltham, MA. Cat. No.: 26620) was used as a molecular weight standard. The gels were run at 120 V for an hour before staining with Coomassie blue (Fisher Scientific, Pittsburgh, PA. Cat. No.: BP101-25) for 10 minutes. Gels were then destained with destaining buffer (10% glacial acetic acid and 10% methanol) overnight before visualization under visible light with an Azure c400 imager (Azure Biosystems, Dublin, CA).

2.6 Size Measurement

TEM samples were prepared for imaging by placing 1.5 μl of the VLP suspension onto formvar/carbon-coated copper grids followed by an equal amount of ACS-grade phosphotungstic acid (PTA, stock concentration: 1%) for negative staining. After 15 sec, the excess liquid was wicked from the grid with 3MM paper, and the grid was allowed to dry. At least 50 images were taken per sample using Tecnai T20 transmission electron microscope (200 kV). More than 20 images with good contrast and focus were analyzed with ImageJ software to measure the dimensions of over 180 nanorods.

Dynamic light scattering was performed with a Malvern Zetasizer Nano ZS instrument. Following 18 days of incubation, 0.40 mL of each sample was placed in triple-rinsed ZEN0040 cuvettes equilibrated to 25 ºC for 30 s before each measurement. The data shown is the average of 10 readings, which were taken for 10 s each at a 173° backscatter measurement angle. Size

distributions were obtained with a general purpose analysis model. All measurements showed good second-order correlation functions with a y-intercept between ~0.9 and 1.

2.7 Measurement of reaction kinetics between BSMV-D101R/199K VLPs and fluorescamine

BSMV-D101R/199K VLPs suspended in 0.01 M HEPES buffer at pH 7.2 were divided into three aliquots. Each aliquot was buffer-exchanged thrice with 0.1 M pH 5 citrate buffer, 1x PBS (pH 7), and 0.1 M pH 9 carbonate-bicarbonate buffer, respectively, using Amicon® Ultra centrifugal filter units with 100 kDa MWCO (MilliporeSigma, Burlington, MA). Stock solution of fluorescamine (concentration: 3.6 mM) was prepared by dissolving 250 mg of fluorescamine powder (Sigma-Aldrich, St. Louis, MO. Cat. No: F9015-250MG) in 25 mL of anhydrous DMSO (Fisher Scientific, Pittsburgh, PA. Cat. No.: AC326880010). VLPs at pH 5, 7, and 9 were mixed with fluorescamine in a 1:100 VLP:fluorescamine molar ratio in a Nunc™ black/clear bottom 96-well plate (Thermo Fisher Scientific, Waltham, MA. Cat. No. 265301). Buffers at corresponding pH were used as blanks. Fluorescence at each time point was measured using a microplate reader (SpectraMax iD5, Molecular Devices, Downingtown, PA) at an excitation wavelength of 380 nm and emission wavelength of 470 nm. Blank subtracted fluorescence intensity values were then plotted against time. Fluorescence measurements were performed in triplicate. Error bars in the graph represent the standard error of mean fluorescence intensities.

2.8 Identification of solvent exposed lysine residues in BSMV

BSMV capsid protein sequence was obtained from UniProt (PDB: 5a7a). A predictive model of D101R coat protein dimers was computed using AlphaFold2 [37]. The models were analyzed using Swiss PDB Viewer (also known as DeepView). Accessible residues were identified by setting accessibility threshold to 50%.

3. Results and Discussion

3.1 Novel residues identified in the BSMV Caspar carboxylate cluster (CCC)

There are various approaches to stabilize rod-shaped plant viruses such as TMV and BSMV, whose structures were recently resolved [16,38]. For example, cysteine insertions enabled

disulfide bond formation between coat proteins, yielding stable TMV nanorods up to pH 11 [39]. While these made efficient catalysts for alkaline hydrogen evolution [40], disruption by reducing agents restricts applicability to electroless metal deposition [41] and intracellular applications [42,43]. Therefore, we thus sought to stabilize BSMV via CCC engineering, another proven strategy for TMV [44]. Crystallization and structural elucidation of chimeric BSMV VLPs revealed close axial contacts between the carboxylate residues on adjacent capsid proteins located at Glu37 (E37), Asp70 (D70), and D74 that have been proposed as the CCC (Figure 1A) [15]. E37 is hypothesized to interact with both D70 and D74 on adjacent capsid proteins; thus, point mutations of E37 to a neutral (Gln/Q) or positive (Arg/R) residue may be sufficient to neutralize the CCC repulsion and stabilize VLPs at alkaline pH. To evaluate their role in assembly, we expressed transcripts encoding BSMV capsid protein point mutants in *E.coli*.

SDS-PAGE analysis confirmed successful heterologous expression of mutant BSMV CPs (Figure S1). Surprisingly, however, the neutral (E37Q) and positive (E37R) mutants did not result in the formation of VLP rods (Figures 1B and 1C). Analogous single point mutations in TMV (e.g., E50Q) resulted in VLP rods and reduced disassembly at elevated pH [11]. These results suggest that E37 is not an amenable site to neutralize repulsive CCC interactions. The suggested CCC residues (E37, D70, and D74) have been shown to be very close to the salt bridge formed between D44 and R69 [15]. Point mutations of residue E37 may have disrupted the salt bridge, thus preventing self-assembly. Structural analyses did not identify alternate interacting residues for the rest of the putative CCC (D70, D74). Thus, we pursued an alternate structure-guided approach based on the structural similarities between TMV and BSMV capsid proteins [15].

Superposition of BSMV and TMV capsid protein crystal structure revealed that D70 and three novel residues (E62, D68, and D101) closely aligned with established TMV CCC residues (Figure 2). D101 of BSMV corresponds to E50 of TMV, while E62, D68, or D70 of BSMV is analogous to D77 of TMV (Figures 2A and 2B). To evaluate this new CCC as a candidate for VLP stabilization, we mutated the negative aspartate (D) to neutral asparagine (N) and negative glutamate (E) to neutral glutamine (Q) or positive arginine (R) through site-directed mutagenesis. Neither D68N nor D70N resulted in the formation of nanorod-shaped VLP (Figure S2). In contrast, E62Q and D101N successfully led to clear, rod-shaped capsid protein assembly (Figure 3A and 3B). Thus, E62 and D101 form a previously unrecognized BSMV CCC that tolerates site-directed mutagenesis for potential stabilization. Combining these mutations also resulted in successful VLP

assembly (Figure 3C). Our results validate the role of E62 and D101 contacts in BSMV self-assembly and demonstrate that these protein::protein interactions can be engineered to stabilize assembly of BSMV VLPs.

We hypothesized that replacing the repulsive negative CCC interactions with attractive, positive/negative interactions will have a strong stabilizing effect on particle assembly. To test this hypothesis, we mutated D101 with positively charged residues such as arginine or lysine that can attract the negative charge of the opposing glutamate. Although D101K did not result in observable VLPs (Figure S3), D101R mutants clearly formed viable VLP rods (Figure 4). The assembly of D101R mutants into VLPs can be attributed to geometric effects of residues. Arginine contains a guanidinium group that allows formation of three salt-bridge and hydrogen bonds, whereas the amino group in lysine allows only one such interaction [45,46]. Stronger electrostatic interactions and improved stability in proteins generated by arginine have been demonstrated indirectly by illustrating higher number of salt-bridges in the presence of arginine than lysine [47,48]. These results validate our hypothesis and suggest that residue geometry and position, and not only charge, are critical for stabilizing interactions between the capsid protein subunits.

3.2 BSMV CCC mutants have enhanced stability under alkaline conditions

BSMV-D101R VLPs were expected to be the most stable mutants generated due to the stronger electrostatic attraction between oppositely charged residues than charge-neutral interactions.[49] We therefore analyzed BSMV-wildtype and BSMV-D101R VLPs under neutral and alkaline conditions to test for stabilized self-assembly. We isolated BSMV-VLP pellets and resuspended them by continuous agitation in 0.1M Tris-HCl at either pH 7 or 9 for 24 h, followed by transmission electron microscopy (TEM) for characterization. TEM images indicate the presence of rod-shaped particles for both wildtype and D101R mutants at pH 7 and 9. TMV literature suggests that non-acidic pH leads to partial disassembly of TMV nanorods [10,50]. Our ImageJ analysis of the TEM images is consistent with this expectation; showing a higher average rod length for D101R (125 nm) than wildtype BSMV VLPs (62 nm) at neutral pH (Figure 4). Notably, there was a similar, ~2-fold difference in alkaline conditions, with D101R having an average rod length of 91 nm and wildtype BSMV VLPs having an average length of 40 nm (Figure 5). These results were consistent with DLS data. The mutant D101R VLPs do not show a clear shift, although a small tail appears at lower sizes at pH 9 (Figure 6A). However, wildtype VLPs

show a leftward shift in the size distribution upon alkaline incubation (Figure 6B). Notably, the wildtype samples show a distinctly large peak at lower sizes, regardless of pH, indicating that they have a larger fraction of (partially) disassembled rods and/or disks multimers. The longer rods in D101R mutants than wildtype VLPs at both pH 7 and 9 indicate that attractive electrostatic interactions play a major role in stabilizing BSMV-D101R-VLPs. Furthermore, their greater range of length and aspect ratio may promote alkaline applications such as pancreatic drug delivery.[51] Alkaline stability also favors efficient inorganic coating, [27,52] ultimately aiding the development of solar cells [53], tough nanocomposites [54], and other technologies that use rod-shaped metal nanoparticle fillers.

After validating our hypothesis that replacing the CCC with a positively-charged residue would have a strong stabilizing effect in neutral and alkaline conditions, we sought to check the assembly state in acidic conditions. Although wildtype VLPs are known to form rod-shaped particles at acidic pH [55], we expected D101R mutants to be relatively destabilized around pH 4, as the glutamate residue (E62) has a pKa of 4.15 [56]. Thus, the interaction residue pair would switch from positive/negative to positive/neutral, leading to reduced attraction. However, TEM images confirmed that BSMV-D101R-VLPs, like the wildtype BSMV VLPs, remain assembled at pH 4 (Figure 7, S4, and S5). The positive/neutral charge of the glutamate side chain at pH 4 still resulted in the presence of rods, which mirrors the assembly of wildtype VLPs with neutral/negative interactions at this condition. These results demonstrate the stability of BSMV-D101R VLPs over a wide range of pH, thus providing an ideal platform for further engineering, such as surface functionalization.

3.3 BSMV mutants can be decorated with primary amines for rapid alkaline surface functionalization

Cryo-electron microscopy elucidation of BSMV capsid protein and virion structure shows particle surface-exposed C-termini (Figure 8A) [15], which provides a site to incorporate functional groups for subsequent chemical modification. To test if the D101R VLP mutant assembly can tolerate single amino acid insertions at the C-terminus, we performed site-directed mutagenesis of the D101R construct to insert a lysine residue at the C-terminus (BSMV-D101R/199K) and expressed the transcripts in *E.coli*. SDS-PAGE analysis shows successful

heterologous expression of the BSMV-D101R/199K coat proteins (Figure S6). The assembly of the modified D101R/199K capsid proteins into rods was validated by TEM images (Figure 8B).

Owing to the versatile pH stability of BSMV-D101R VLPs, D101R/199K VLPs were used to study the kinetics of the labeling reaction at acidic, neutral, and alkaline conditions. Reaction between surface-exposed lysine residues and fluorescamine (Figure 9A) showed faster kinetics at neutral and alkaline pH than acidic pH (Figure 9B), which took over 41 times as long to reach completion. The fluorescence intensity of the resulting fluorophore is known to stay constant between pH 4.5 and 10.5 [57]; thus, the measured fluorescence intensity serves as a proxy for the extent of reaction. The trends are as expected; the side chain amines in lysine would be protonated at pH 5, resulting in lower reactivity than VLPs in neutral and alkaline pH. As the unprotonated amines react with fluorescamine, the reaction equilibrium will shift towards more amines getting unprotonated, thus validating the increase in fluorescence intensity with time at pH 5. The reaction between fluorescamine and amine groups reaches the maximum within 10 min for both pH 7 and 9 and matches the pH conditions typically used for conjugation reactions with lysine residues [58]. These results indicate that BSMV-D101R VLP mutants can serve as a pH-stable platform for surface functionalization, thus providing opportunities for use in numerous applications.

Surface functionalization strategies are well-established for some, but not all, plant viruses [29]. Popular viruses such as TMV and potato virus X, which claim the majority of research focus on rod-shaped plant viruses in recent decades, have been decorated with a wide array of small molecules, polymers, metals, peptides, proteins, and various other ligands through chemical and biomolecular approaches [9,59]. However, barley stripe mosaic virus (BSMV) has recently emerged as a potentially more powerful tool for synthesis of metallic biohybrid nanomaterials [17]. BSMV and TMV belong to the *Virgaviridae* family of viruses and share many structural features and a similar assembly mechanism [16,60]. The surface of BSMV appears to be more active than TMV, however, encoding additional electrostatic interactions that result in more dense, rapid, and uniform coating with metals such as palladium [24]. Systematic surface engineering to understand and further improve BSMV's superior coating properties may lead to more efficient coating processes for the development of more sensitive sensors and higher capacity batteries. By genetically modifying BSMV VLPs for surface display for the first time, we enable these future efforts. Our successful lysine insertion will also facilitate diverse surface modifications through amine chemistry to further develop BSMV VLPs as a biotemplate for nanomaterial synthesis. Our

bacterial expression system enables flexible protein engineering, which should be leveraged in future work for the surface functionalization of BSMV VLPs with new residues, peptides, and proteins for broader applications.

4. Conclusions

We demonstrate *in vivo* production of recombinant BSMV VLPs engineered for alkaline stability and surface modification via amine couplings. Novel BMV Caspar carboxylate cluster residues are identified through atomic modeling, examined systematically, and leveraged for protein engineering. By introducing positive point mutations on selective carboxylate residues, changes in internal protein-protein interactions drive the rod-shaped assembly of BSMV capsid proteins and lead to increased nanorod stability. These synthesized virus-like particles show enhanced structural integrity under atypical processing conditions, at pH values up to 9. We further modify these stabilized mutants to display lysine residues at the VLP surface and demonstrate that its reactive amino functional group can be leveraged for chemical modifications. Overall, this work represents an important step towards the development of BSMV VLPs as a platform for surface functionalization with diverse applications in nanotechnology.

CRediT authorship contribution statement

Akash J. Vaidya: Conceptualization, Methodology, Validation, Formal analysis, Investigation, Writing - Original Draft, Writing - Review & Editing, Visualization. **Mruthula Rammohan:** Conceptualization, Methodology, Validation, Formal analysis, Investigation, Writing - Original Draft, Writing - Review & Editing, Visualization. **Yu-Hsuan Lee:** Conceptualization, Validation, Formal analysis, Investigation, Writing - Original Draft, Visualization. **Kok Zhi Lee:** Conceptualization, Methodology, Validation, Formal analysis, Investigation, Resources, Writing - Original Draft, Visualization. **Che-Yu Chou:** Investigation**. Zachary Hartley:** Investigation. **Corren A. Scott:** Investigation. **Rachel G. Susler:** Investigation. **Longfei Wang: L.** Investigation**. Sue Loesch-Fries:** Supervision, Project administration, Funding acquisition. **Michael T. Harris:** Supervision, Project administration, Funding acquisition. **Kevin V. Solomon:** Conceptualization, Writing - Review & Editing, Supervision, Project administration, Funding acquisition.

Declaration of Competing Interest

The authors declare that they have no known competing financial interests or personal relationships that could have appeared to influence the work reported in this paper.

Funding

This material is based upon work supported by the National Science Foundation under Grant No. CBET-2028618/CBET-2219276 and by the Delaware INBRE program, with a grant from the National Institute of General Medical Sciences – NIGMS (P20 GM103446) from the National Institutes of Health and the State of Delaware. The research was also supported by the Robert B. and Virginia V. Covalt Professorship of Chemical Engineering, the Purdue Department of Botany & Plant Pathology, the Purdue Research Foundation (Fellowships #60000025 & #60000029) and the USDA National Institute of Food and Agriculture (Hatch Multistate Project S1075).

Acknowledgments

We would like to gratefully thank Dr. James Culver at the University of Maryland Biotechnology Institute, Center for Biosystems Research, for his insights on the production of VLPs, and Electron microscopy was performed with the help of Dr. Christopher J. Gilpin, Laurie Mueller, and Robert Seiler in the Purdue Life Science Microscopy Facility, and the University of Delaware Advanced Materials Characterization Laboratory.

REFERENCES

[1] Y. Zhang, Y. Dong, J. Zhou, X. Li, F. Wang, Application of Plant Viruses as a Biotemplate for Nanomaterial Fabrication, Molecules. 23 (2018) 2311. https://doi.org/10.3390/molecules23092311.

[2] K.-B.G. Scholthof, S. Adkins, H. Czosnek, P. Palukaitis, E. Jacquot, T. Hohn, B. Hohn, K. Saunders, T. Candresse, P. Ahlquist, C. Hemenway, G.D. Foster, Top 10 plant viruses in molecular plant pathology, Molecular Plant Pathology. 12 (2011) 938–954. https://doi.org/10.1111/j.1364-3703.2011.00752.x.

[3] A.M.Q. King, M.J. Adams, E.B. Carstens, E.J. Lefkowitz, eds., Part II. The Viruses, in: Virus Taxonomy, Elsevier, San Diego, 2012: pp. 21–36. https://doi.org/10.1016/B978-0-12-384684-6.00115-4.

[4] S. Nooraei, H. Bahrulolum, Z.S. Hoseini, C. Katalani, A. Hajizade, A.J. Easton, G. Ahmadian, Virus-like particles: preparation, immunogenicity and their roles as nanovaccines and drug nanocarriers, J Nanobiotechnology. 19 (2021) 59. https://doi.org/10.1186/s12951-021-00806-7.

[5] N.A. Nikitin, E.A. Trifonova, O.V. Karpova, J.G. Atabekov, Biosafety of plant viruses for human and animals, Moscow Univ. Biol.Sci. Bull. 71 (2016) 128–134. https://doi.org/10.3103/S0096392516030081.

[6] J.N. Culver, A.D. Brown, F. Zang, M. Gnerlich, K. Gerasopoulos, R. Ghodssi, Plant virus directed fabrication of nanoscale materials and devices, Virology. 479–480 (2015) 200–212. https://doi.org/10.1016/j.virol.2015.03.008.

[7] E.A. Evtushenko, E.M. Ryabchevskaya, N.A. Nikitin, J.G. Atabekov, O.V. Karpova, Plant virus particles with various shapes as potential adjuvants, Sci Rep. 10 (2020) 10365. https://doi.org/10.1038/s41598-020-67023-4.

[8] K.L. Hefferon, Repurposing Plant Virus Nanoparticles, Vaccines. 6 (2018) 11. https://doi.org/10.3390/vaccines6010011.

[9] K.Z. Lee, V.B. Pussepitiyalage, Y.-H. Lee, L.S. Loesch-Fries, M.T. Harris, S. Hemmati, K.V. Solomon, Engineering Tobacco Mosaic Virus and Its Virus-Like-Particles for Synthesis of Biotemplated Nanomaterials, Biotechnology Journal. 16 (2021) 2000311. https://doi.org/10.1002/biot.202000311.

[10] W.K. Kegel, P. van der Schoot, Physical Regulation of the Self-Assembly of Tobacco Mosaic Virus Coat Protein, Biophysical Journal. 91 (2006) 1501–1512. https://doi.org/10.1529/biophysj.105.072603.

[11] J.N. Culver, W.O. Dawson, K. Plonk, G. Stubbs, Site-directed mutagenesis confirms the involvement of carboxylate groups in the disassembly of tobacco mosaic virus, Virology. 206 (1995) 724–730.

[12] B. Lu, G. Stubbs, J.N. Culver, Carboxylate interactions involved in the disassembly of tobacco mosaic tobamovirus, Virology. 225 (1996) 11–20. https://doi.org/10.1006/viro.1996.0570.

[13] B. Lu, F. Taraporewala, G. Stubbs, J.N. Culver, Intersubunit interactions allowing a carboxylate mutant coat protein to inhibit tobamovirus disassembly, Virology. 244 (1998) 13–19. https://doi.org/10.1006/viro.1998.9099.

[14] A.C.H. Durham, J.T. Finch, A. Klug, States of Aggregation of Tobacco Mosaic Virus Protein, Nature New Biology. 229 (1971) 37–42. https://doi.org/10/gnzjcm.

[15] D.K. Clare, E.V. Pechnikova, E.V. Skurat, V.V. Makarov, O.S. Sokolova, A.G. Solovyev, E.V. Orlova, Novel inter-subunit contacts in barley stripe mosaic virus revealed by cryo-electron microscopy, Structure. 23 (2015) 1815–1826.
[16] D.K. Clare, E.V. Pechnikova, E.V. Skurat, V.V. Makarov, O.S. Sokolova, A.G. Solovyev, E.V. Orlova, Novel Inter-Subunit Contacts in Barley Stripe Mosaic Virus Revealed by Cryo-Electron Microscopy, Structure. 23 (2015) 1815–1826. https://doi.org/10.1016/j.str.2015.06.028.
[17] O.O. Adigun, E.L. Retzlaff-Roberts, G. Novikova, L. Wang, B.-S. Kim, J. Ilavsky, J.T. Miller, L.S. Loesch-Fries, M.T. Harris, BSMV as a biotemplate for palladium nanomaterial synthesis, Langmuir. 33 (2017) 1716–1724.
[18] A.J. Vaidya, K.V. Solomon, Surface Functionalization of Rod-Shaped Viral Particles for Biomedical Applications, ACS Appl. Bio Mater. (2022) acsabm.1c01204. https://doi.org/10.1021/acsabm.1c01204.
[19] S. Werner, S. Marillonnet, G. Hause, V. Klimyuk, Y. Gleba, Immunoabsorbent nanoparticles based on a tobamovirus displaying protein A, PNAS. 103 (2006) 17678–17683. https://doi.org/10.1073/pnas.0608869103.
[20] D. Carignan, A. Thérien, G. Rioux, G. Paquet, M.-È.L. Gagné, M. Bolduc, P. Savard, D. Leclerc, Engineering of the PapMV vaccine platform with a shortened M2e peptide leads to an effective one dose influenza vaccine, Vaccine. 33 (2015) 7245–7253. https://doi.org/10.1016/j.vaccine.2015.10.123.
[21] J. Denis, E. Acosta-Ramirez, Y. Zhao, M.-E. Hamelin, I. Koukavica, M. Baz, Y. Abed, C. Savard, C. Pare, C. Lopez Macias, G. Boivin, D. Leclerc, Development of a universal influenza A vaccine based on the M2e peptide fused to the papaya mosaic virus (PapMV) vaccine platform, Vaccine. 26 (2008) 3395–3403. https://doi.org/10.1016/j.vaccine.2008.04.052.
[22] M.L. Smith, J.A. Lindbo, S. Dillard-Telm, P.M. Brosio, A.B. Lasnik, A.A. McCormick, L.V. Nguyen, K.E. Palmer, Modified Tobacco mosaic virus particles as scaffolds for display of protein antigens for vaccine applications, Virology. 348 (2006) 475–488. https://doi.org/10.1016/j.virol.2005.12.039.
[23] C. Wege, F. Geiger, Dual Functionalization of Rod-Shaped Viruses on Single Coat Protein Subunits, in: C. Wege, G.P. Lomonossoff (Eds.), Virus-Derived Nanoparticles for Advanced Technologies: Methods and Protocols, Springer, New York, NY, 2018: pp. 405–424. https://doi.org/10.1007/978-1-4939-7808-3_27.
[24] Y.-H. Lee, K.Z. Lee, R.G. Susler, C.A. Scott, L. Wang, L.S. Loesch-Fries, M.T. Harris, K.V. Solomon, Bacterial Production of Barley Stripe Mosaic Virus Biotemplates for Palladium Nanoparticle Growth, ACS Appl. Nano Mater. 3 (2020) 12080–12086. https://doi.org/10.1021/acsanm.0c02570.
[25] S. Rabindran, W.O. Dawson, Assessment of Recombinants That Arise from the Use of a TMV-Based Transient Expression Vector, Virology. 284 (2001) 182–189. https://doi.org/10/b7v7fz.
[26] M. Ramani, B.S. Haran, R.E. White, B.N. Popov, L. Arsov, Studies on activated carbon capacitor materials loaded with different amounts of ruthenium oxide, Journal of Power Sources. 93 (2001) 209–214. https://doi.org/10.1016/S0378-7753(00)00575-9.
[27] J. Ma, Z. Zhang, Y. Liu, X. Zhang, H. Luo, G. Yao, Pd-Free Activation Pretreatment for Electroless Ni-P Plating on NiFe2O4 Particles, Materials (Basel). 11 (2018) 1810. https://doi.org/10.3390/ma11101810.

[28] Spatially Selective Nucleation of Metal Clusters on the Tobacco Mosaic Virus - Knez - 2004 - Advanced Functional Materials - Wiley Online Library, (n.d.). https://onlinelibrary-wiley-com.udel.idm.oclc.org/doi/10.1002/adfm.200304376 (accessed April 26, 2022).
[29] A.J. Vaidya, K.V. Solomon, Surface Functionalization of Rod-Shaped Viral Particles for Biomedical Applications, ACS Appl. Bio Mater. (2022). https://doi.org/10.1021/acsabm.1c01204.
[30] L. Petri, P. A. Szijj, Á. Kelemen, T. Imre, Á. Gömöry, M.T. W. Lee, K. Hegedűs, P. Ábrányi-Balogh, V. Chudasama, G. Miklós Keserű, Cysteine specific bioconjugation with benzyl isothiocyanates, RSC Advances. 10 (2020) 14928–14936. https://doi.org/10.1039/D0RA02934C.
[31] D. Nolting, E.F. Aziz, N. Ottosson, M. Faubel, I.V. Hertel, B. Winter, pH-Induced Protonation of Lysine in Aqueous Solution Causes Chemical Shifts in X-ray Photoelectron Spectroscopy, J. Am. Chem. Soc. 129 (2007) 14068–14073. https://doi.org/10.1021/ja0729711.
[32] J.N. Culver, W.O. Dawson, K. Plonk, G. Stubbs, Site-directed mutagenesis confirms the involvement of carboxylate groups in the disassembly of tobacco mosaic virus, Virology. 206 (1995) 724–730. https://doi.org/10.1016/s0042-6822(95)80096-4.
[33] A.D. Brown, L. Naves, X. Wang, R. Ghodssi, J.N. Culver, Carboxylate-Directed In Vivo Assembly of Virus-like Nanorods and Tubes for the Display of Functional Peptides and Residues, Biomacromolecules. 14 (2013) 3123–3129. https://doi.org/10.1021/bm400747k.
[34] Y. Zhang, J. Skolnick, TM-align: a protein structure alignment algorithm based on the TM-score, Nucleic Acids Res. 33 (2005) 2302–2309. https://doi.org/10.1093/nar/gki524.
[35] J. Sambrook, E.F. Fritsch, T. Maniatis, Molecular cloning: a laboratory manual, Cold Spring Harbor Laboratory Press, 1989.
[36] J. Braman, C. Papworth, A. Greener, Site-Directed Mutagenesis Using Double-Stranded Plasmid DNA Templates, in: M.K. Trower (Ed.), In Vitro Mutagenesis Protocols, Humana Press, Totowa, NJ, 1996: pp. 31–44. https://doi.org/10.1385/0-89603-332-5:31.
[37] J. Jumper, R. Evans, A. Pritzel, T. Green, M. Figurnov, O. Ronneberger, K. Tunyasuvunakool, R. Bates, A. Žídek, A. Potapenko, A. Bridgland, C. Meyer, S.A.A. Kohl, A.J. Ballard, A. Cowie, B. Romera-Paredes, S. Nikolov, R. Jain, J. Adler, T. Back, S. Petersen, D. Reiman, E. Clancy, M. Zielinski, M. Steinegger, M. Pacholska, T. Berghammer, S. Bodenstein, D. Silver, O. Vinyals, A.W. Senior, K. Kavukcuoglu, P. Kohli, D. Hassabis, Highly accurate protein structure prediction with AlphaFold, Nature. 596 (2021) 583–589. https://doi.org/10.1038/s41586-021-03819-2.
[38] D.K. Clare, E.V. Orlova, 4.6Å Cryo-EM reconstruction of tobacco mosaic virus from images recorded at 300keV on a 4k×4k CCD camera, Journal of Structural Biology. 171 (2010) 303–308. https://doi.org/10.1016/j.jsb.2010.06.011.
[39] K. Zhou, F. Li, G. Dai, C. Meng, Q. Wang, Disulfide Bond: Dramatically Enhanced Assembly Capability and Structural Stability of Tobacco Mosaic Virus Nanorods, Biomacromolecules. 14 (2013) 2593–2600. https://doi.org/10.1021/bm400445m.
[40] K. Zhou, Y. Zhou, H. Yang, H. Jin, Y. Ke, Q. Wang, Interfacially Bridging Covalent Network Yields Hyperstable and Ultralong Virus-Based Fibers for Engineering Functional Materials, Angewandte Chemie. 132 (2020) 18406–18412. https://doi.org/10.1002/ange.202008670.
[41] K.M. Bromley, A.J. Patil, A.W. Perriman, G. Stubbs, S. Mann, Preparation of high quality nanowires by tobacco mosaic virus templating of gold nanoparticles, J. Mater. Chem. 18

(2008) 4796–4801. https://doi.org/10.1039/B809585J.
[42] D. Zhang, A. Fourie-O'Donohue, P.S. Dragovich, T.H. Pillow, J.D. Sadowsky, K.R. Kozak, R.T. Cass, L. Liu, Y. Deng, Y. Liu, C.E.C.A. Hop, S.C. Khojasteh, Catalytic Cleavage of Disulfide Bonds in Small Molecules and Linkers of Antibody–Drug Conjugates, Drug Metab Dispos. 47 (2019) 1156–1163. https://doi.org/10.1124/dmd.118.086132.
[43] Q. Wei, S. He, J. Qu, J. Xia, Synthetic Multienzyme Complexes Assembled on Virus-like Particles for Cascade Biosynthesis *In Cellulo*, Bioconjugate Chem. 31 (2020) 2413–2420. https://doi.org/10.1021/acs.bioconjchem.0c00476.
[44] A.D. Brown, S. Chu, M. Kappagantu, R. Ghodssi, J.N. Culver, Reprogramming Virus Coat Protein Carboxylate Interactions for the Patterned Assembly of Hierarchical Nanorods, Biomacromolecules. 22 (2021) 2515–2523. https://doi.org/10/gnmchn.
[45] C. l. Borders Jr., J.A. Broadwater, P.A. Bekeny, J.E. Salmon, A.S. Lee, A.M. Eldridge, V.B. Pett, A structural role for arginine in proteins: Multiple hydrogen bonds to backbone carbonyl oxygens, Protein Science. 3 (1994) 541–548. https://doi.org/10.1002/pro.5560030402.
[46] J.E. Donald, D.W. Kulp, W.F. DeGrado, Salt bridges: Geometrically specific, designable interactions, Proteins: Structure, Function, and Bioinformatics. 79 (2011) 898–915. https://doi.org/10.1002/prot.22927.
[47] B. Musafia, V. Buchner, D. Arad, Complex Salt Bridges in Proteins: Statistical Analysis of Structure and Function, Journal of Molecular Biology. 254 (1995) 761–770. https://doi.org/10.1006/jmbi.1995.0653.
[48] M. Matsutani, H. Hirakawa, M. Nishikura, W. Soemphol, I.A.I. Ali, T. Yakushi, K. Matsushita, Increased number of Arginine-based salt bridges contributes to the thermotolerance of thermotolerant acetic acid bacteria, Acetobacter tropicalis SKU1100, Biochemical and Biophysical Research Communications. 409 (2011) 120–124. https://doi.org/10.1016/j.bbrc.2011.04.126.
[49] H.-X. Zhou, X. Pang, Electrostatic Interactions in Protein Structure, Folding, Binding, and Condensation, Chem Rev. 118 (2018) 1691–1741. https://doi.org/10.1021/acs.chemrev.7b00305.
[50] H. Yi, S. Nisar, S.-Y. Lee, M.A. Powers, W.E. Bentley, G.F. Payne, R. Ghodssi, G.W. Rubloff, M.T. Harris, J.N. Culver, Patterned Assembly of Genetically Modified Viral Nanotemplates via Nucleic Acid Hybridization, Nano Lett. 5 (2005) 1931–1936. https://doi.org/10.1021/nl051254r.
[51] M. Cooley, A. Sarode, M. Hoore, D. A. Fedosov, S. Mitragotri, A.S. Gupta, Influence of particle size and shape on their margination and wall-adhesion: implications in drug delivery vehicle design across nano-to-micro scale, Nanoscale. 10 (2018) 15350–15364. https://doi.org/10.1039/C8NR04042G.
[52] M. Ramani, B.S. Haran, R.E. White, B.N. Popov, L. Arsov, Studies on activated carbon capacitor materials loaded with different amounts of ruthenium oxide, Journal of Power Sources. 93 (2001) 209–214. https://doi.org/10.1016/S0378-7753(00)00575-9.
[53] V.T. Pham, M. Dutta, H.T. Bui, N. Fukata, Effect of nanowire length on the performance of silicon nanowires based solar cell, Adv. Nat. Sci: Nanosci. Nanotechnol. 5 (2014) 045014. https://doi.org/10.1088/2043-6262/5/4/045014.
[54] A. Kutvonen, G. Rossi, S.R. Puisto, N.K.J. Rostedt, T. Ala-Nissila, Influence of nanoparticle size, loading, and shape on the mechanical properties of polymer

nanocomposites, The Journal of Chemical Physics. 137 (2012) 214901. https://doi.org/10.1063/1.4767517.
[55] B.D. Harrison, T.M.A. Wilson, A. Klug, The tobacco mosaic virus particle: structure and assembly, Philosophical Transactions of the Royal Society of London. Series B: Biological Sciences. 354 (1999) 531–535. https://doi.org/10.1098/rstb.1999.0404.
[56] CRC Handbook of Chemistry and Physics, 87th ed Editor-in-Chief: David R. Lide (National Institute of Standards and Technology). CRC Press/Taylor and Francis Group: Boca Raton, FL. 2006. 2608 pp. $139.95. ISBN 0-8493-0487-3., J. Am. Chem. Soc. 129 (2007) 724–724. https://doi.org/10.1021/ja069813z.
[57] S. De Bernardo, M. Weigele, V. Toome, K. Manhart, W. Leimgruber, P. Böhlen, S. Stein, S. Udenfriend, Studies on the reaction of fluorescamine with primary amines, Archives of Biochemistry and Biophysics. 163 (1974) 390–399. https://doi.org/10.1016/0003-9861(74)90490-1.
[58] M. Brinkley, A brief survey of methods for preparing protein conjugates with dyes, haptens and crosslinking reagents, Bioconjugate Chem. 3 (1992) 2–13. https://doi.org/10.1021/bc00013a001.
[59] K.L. Lee, K. Uhde-Holzem, R. Fischer, U. Commandeur, N.F. Steinmetz, Genetic Engineering and Chemical Conjugation of Potato Virus X, Methods Mol Biol. 1108 (2014) 3–21. https://doi.org/10.1007/978-1-62703-751-8_1.
[60] K.Z. Lee, V.B. Pussepitiya, Y.H. Lee, S.L. Fries, M. Harris, S. Hemmati, K. Solomon, Engineering Tobacco Mosaic Virus, Barley Stripe Mosaic Virus, and their Virus-Like-Particles for Synthesis of Biotemplated Nanomaterials, Preprints, 2020. https://doi.org/10.22541/au.159414778.89024447.

Figure 1. Mutating CCC residues predicted by cyro-EM prevents VLP assembly. (A) Residues E37,D70, and D74 in BSMV and transmission electron microscope images of mutants (B) E37Q and (C) E37R.

Figure 2. Potential Caspar carboxylate cluster (CCC) carboxylates in BSMV. (A) Caspar carboxylate cluster of TMV (PDB:2xea) and (B) proposed candidate residues (E62, D68, D70, and D101) in BSMV (PDB:5a7a) based on structural alignment, and (C) their overlay. Predicted CCC is based on crystal structure literature [15].

Figure 3. **Mutating CCC residues predicted by structural overlay allows VLP assembly.** Transmission electron microscope images of BSMV-CP single mutants (A) E62Q (B) D101N, and (C) double mutant E62Q/D101N

Figure 4. D101R mutant VLPs are stabilized in neutral conditions. Transmission electron microscope image of (A) wildtype BSMV VLPs and (B) mutant BSMV-D101R VLPs with its (C) corresponding length distributions at pH 7.

Figure 5. D101R mutant VLPs are stabilized in alkaline conditions. Transmission electron microscope image of (A) wildtype BSMV VLPs and (B) mutant BSMV-D101R with its (C) corresponding length distributions at pH 9.

Figure 6. **D101R mutants have a reduced fraction of disassembled rods**. Dynamic light scattering of (A) D101R mutant VLPs and (B) wildtype BSMV VLPs

Figure 7. D101R mutant VLPs assemble in acidic conditions. Transmission electron microscope image of (A) wildtype BSMV VLPs and (B) mutant BSMV-D101R VLPs at pH 4.

Figure 8. Surface display of lysine residue on D101R mutant VLPs. (A) Cryo-electron microscope elucidated structure of BSMV virion with surface-exposed C-termini [15] (B) Transmission electron microscope image of BSMV-D101R/199K VLPs

Figure 9. Reaction between solvent-exposed primary amines on D101R 199K mutants and fluorescamine occur faster at neutral and alkaline conditions than acidic conditions. (A) Schematic of the reaction between primary amine and fluorescamine. (B) Graph showing the fluorescence intensity of fluorophore-conjugated primary amines at pH 5, 7, and 9. Error bars represent standard error of measurements performed in triplicate.

Figure 1

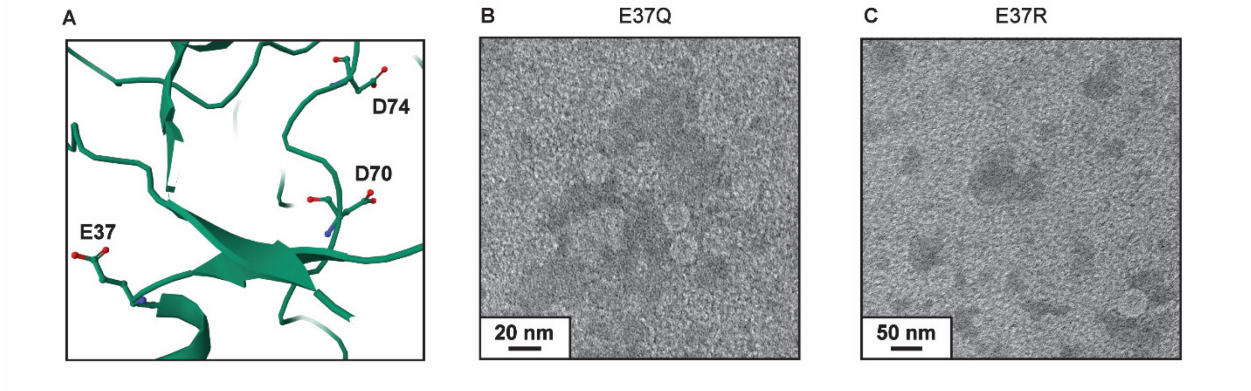

Figure 2

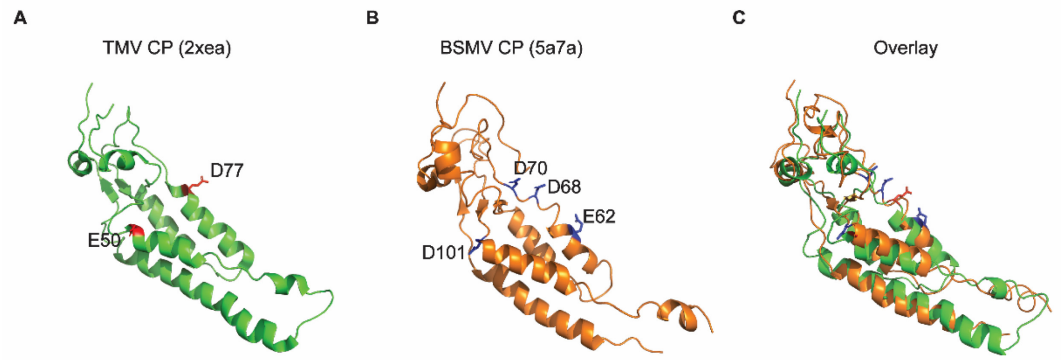

Figure 3

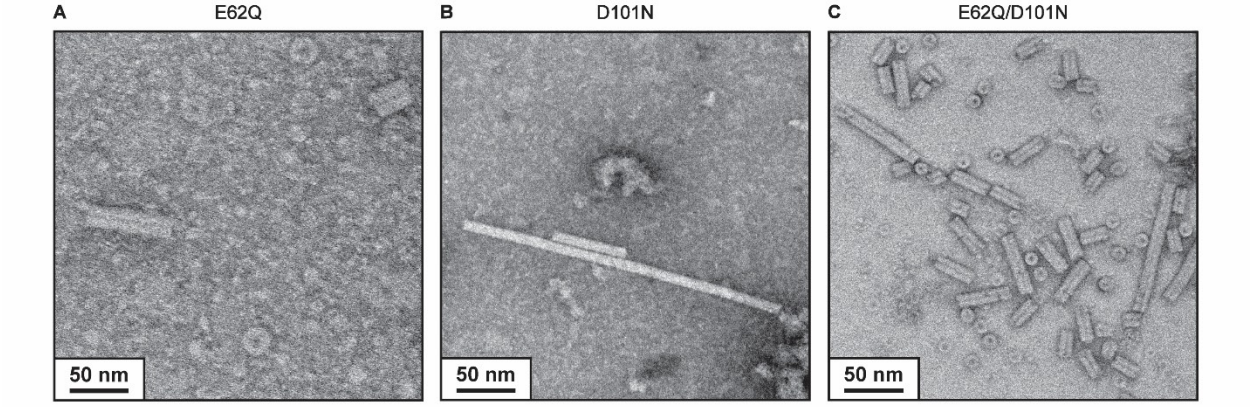

Figure 4

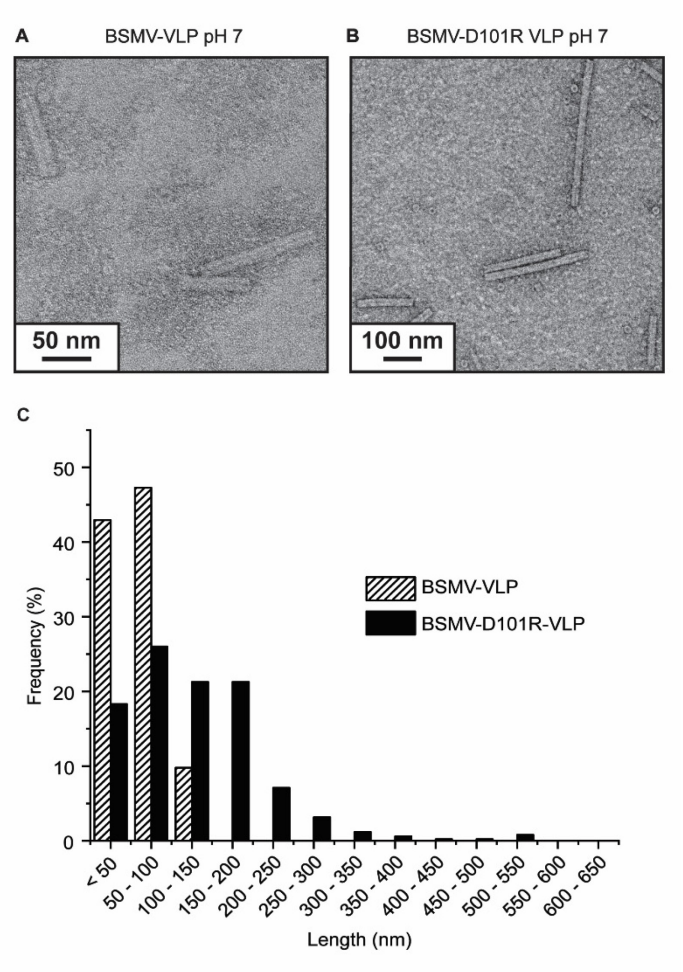
A
BSMV-VLP pH 7
B
BSMV-D101R VLP pH 7
50 nm
100 nm
C
Frequency (%)
0
10
20
30
40
50
BSMV-VLP
BSMV-D101R-VLP
< 50
50 - 100
100 - 150
150 - 200
200 - 250
250 - 300
300 - 350
350 - 400
400 - 450
450 - 500
500 - 550
550 - 600
600 - 650
Length (nm)

507 **Figure 5**

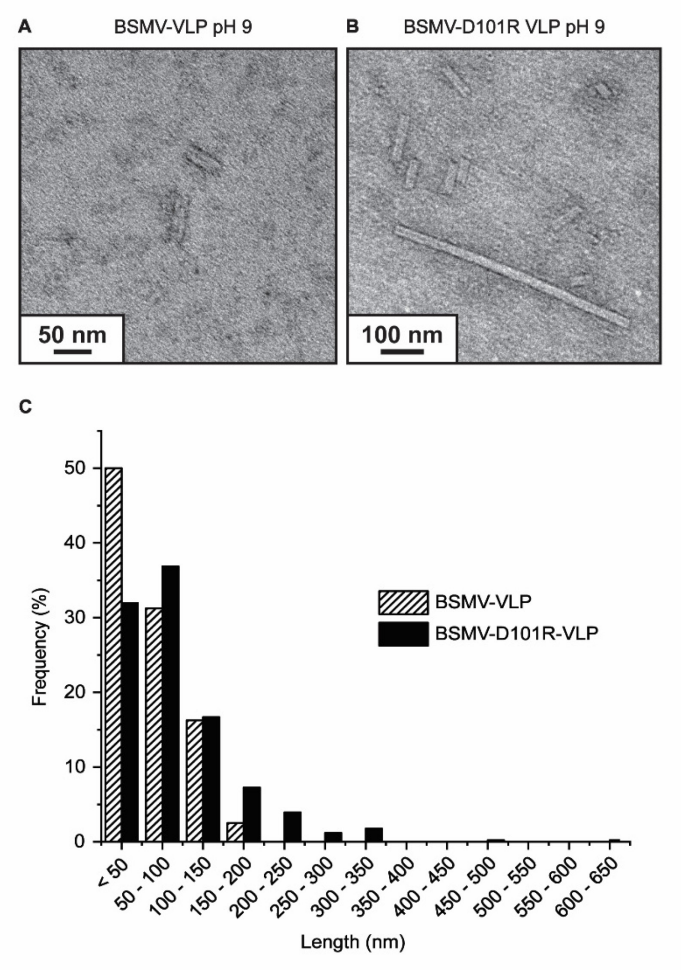

508
509

Figure 6

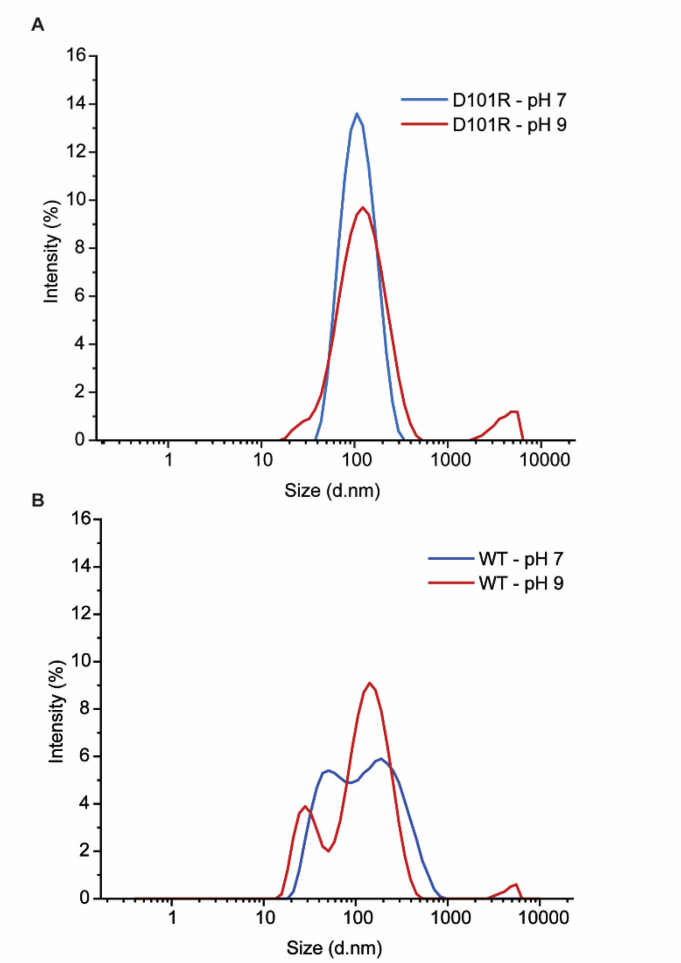

Figure 7

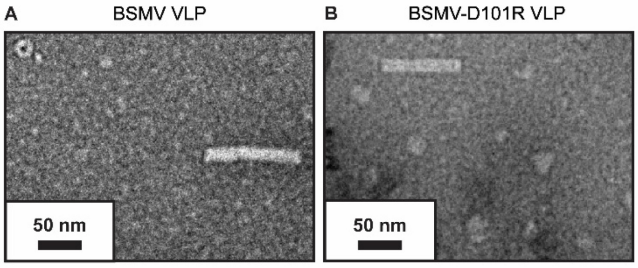

516 **Figure 8**

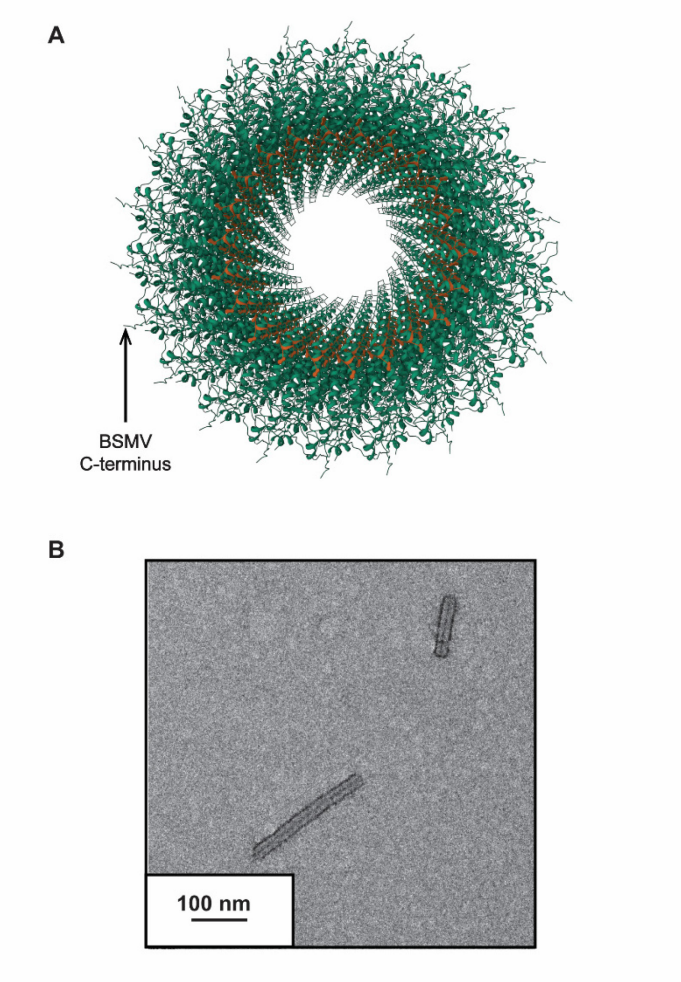

517
518

519 **Figure 9**

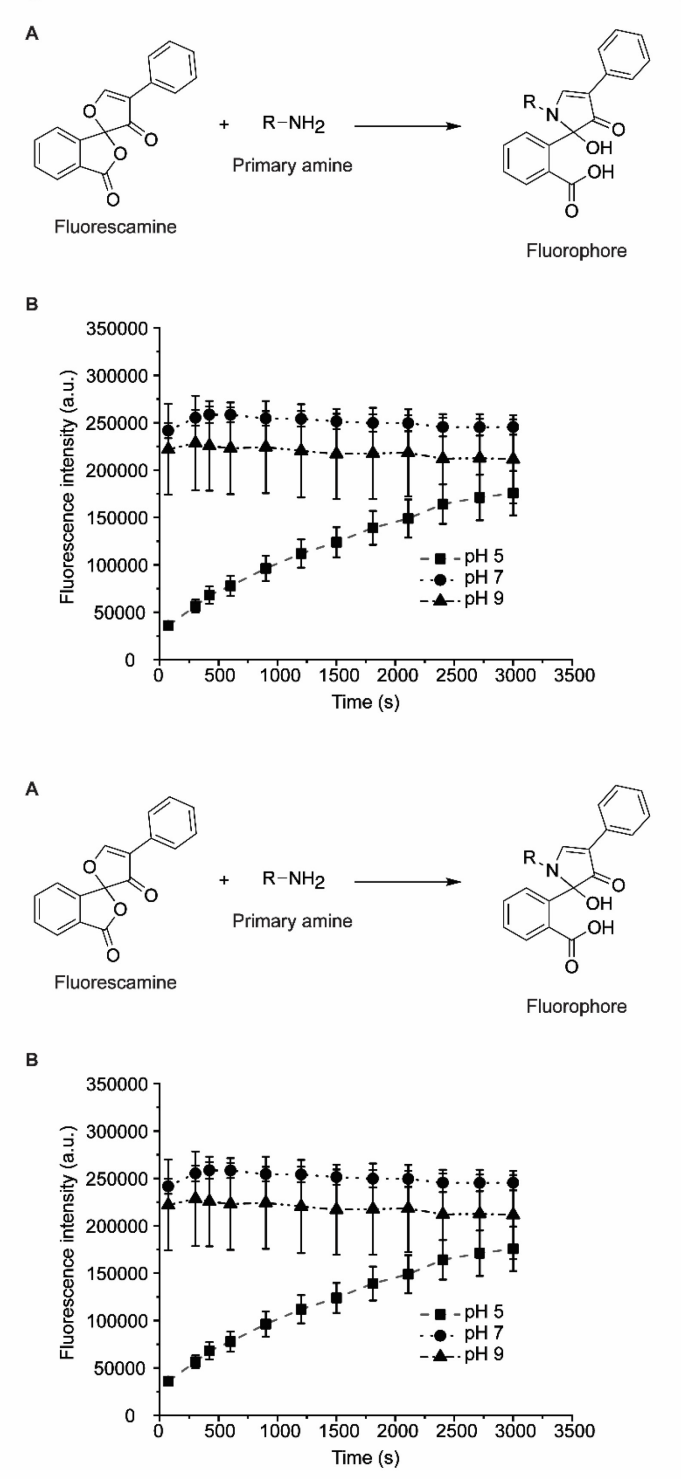

520

A
+ R–NH2
Primary amine
Fluorescamine
Fluorophore
B
Fluorescence intensity (a.u.)
Time (s)
pH 5
pH 7
pH 9

521
522